

UC Riverside

UC Riverside Previously Published Works

Title

PANDORA-Seq unveilsthe hidden small noncoding RNA landscape in atherosclerosis of LDL receptor-deficient mice

Permalink

<https://escholarship.org/uc/item/9901502z>

Journal

Journal of Lipid Research, 64(4)

ISSN

0022-2275

Authors

Hernandez, Rebecca
Shi, Junchao
Liu, Jingwei
[et al.](#)

Publication Date

2023-04-01

DOI

10.1016/j.jlr.2023.100352

Peer reviewed



PANDORA-Seq unveils the hidden small noncoding RNA landscape in atherosclerosis of LDL receptor-deficient mice

Rebecca Hernandez^{1,‡}, Junchao Shi^{1,‡}, Jingwei Liu¹, Xiuchun Li¹, Jake Wu¹, Linlin Zhao², Tong Zhou³, Qi Chen^{1,4}, and Changcheng Zhou^{1,*}

¹Division of Biomedical Sciences, School of Medicine, and ²Department of Chemistry, University of California, Riverside, CA, USA; ³Department of Physiology and Cell Biology, Reno School of Medicine, University of Nevada, Reno, NV, USA; ⁴Molecular Medicine Program, Division of Urology, Department of Surgery, University of Utah School of Medicine, Salt Lake City, UT, USA

Abstract Small noncoding RNAs (sncRNAs) play diverse roles in numerous biological processes. While the widely used RNA sequencing (RNA-Seq) method has advanced sncRNA discovery, RNA modifications can interfere with the complementary DNA library construction process, preventing the discovery of highly modified sncRNAs including transfer RNA-derived small RNAs (tsRNAs) and ribosomal RNA-derived small RNAs (rsRNAs) that may have important functions in disease development. To address this technical obstacle, we recently developed a novel PANDORA-Seq (Panoramic RNA Display by Overcoming RNA Modification Aborted Sequencing) method to overcome RNA modification-elicited sequence interferences. To identify novel sncRNAs associated with atherosclerosis development, LDL receptor-deficient ($LDLR^{-/-}$) mice were fed a low-cholesterol diet or high-cholesterol diet (HCD) for 9 weeks. Total RNAs isolated from the intima were subjected to PANDORA-Seq and traditional RNA-Seq. By overcoming RNA modification-elicited limitations, PANDORA-Seq unveiled an rsRNA/tsRNA-enriched sncRNA landscape in the atherosclerotic intima of $LDLR^{-/-}$ mice, which was strikingly different from that detected by traditional RNA-Seq. While microRNAs were the dominant sncRNAs detected by traditional RNA-Seq, PANDORA-Seq substantially increased the reads of rsRNAs and tsRNAs. PANDORA-Seq also detected 1,383 differentially expressed sncRNAs induced by HCD feeding, including 1,160 rsRNAs and 195 tsRNAs. One of HCD-induced intimal tsRNAs, tsRNA-Arg-CCG, may contribute to atherosclerosis development by regulating the proatherogenic gene expression in endothelial cells. **■** Overall, PANDORA-Seq revealed a hidden rsRNA and tsRNA population associated with atherosclerosis development. These understudied tsRNAs and rsRNAs, which are much more abundant than microRNAs in the atherosclerotic

intima of $LDLR^{-/-}$ mice, warrant further investigations.

Supplementary key words small noncoding RNA • atherosclerosis • cardiovascular disease • tRNA-derived small RNA • rRNA-derived small RNA • PANDORA-Seq • dyslipidemia • transcriptome • vascular biology

Atherosclerosis is a chronic inflammatory disease characterized by the accumulation of cholesterol, immune cells, and fibrous elements in the subintimal layer of the artery leading to plaque formation and cardiovascular events (1–5). At the cellular level, the initial stages of atherosclerosis development involve endothelial dysfunction followed by macrophage infiltration, lipid accumulation, and vascular smooth muscle cell (SMC) migration into the intimal layer of the vasculature (1, 2, 6). While many cell types contribute to atherosclerosis (6–9), endothelial cells in the intimal layer are critical for atherosclerosis initiation and progression (6). Many genetic and environmental factors have been identified to contribute to atherosclerosis development and endothelial dysfunction (10), such as environmental pollutants (11–14) and diet (15). In addition to well-defined risk factors, numerous noncoding RNAs (ncRNAs), such as long ncRNAs and small noncoding RNAs (sncRNAs), have been shown to play important roles in regulating atherosclerosis development (16–20). For example, several long ncRNAs including MALAT1 and VINAS have been demonstrated to regulate atherosclerosis development (16, 19, 20).

For sncRNAs, most studies in the atherosclerosis research field focus on the functions of microRNAs (miRNAs) in atherogenesis (16–18). In addition to

[‡]These authors contributed equally to this work.

*For correspondence: Changcheng Zhou, changcheng.zhou@ucr.edu.

miRNAs, there are many other sncRNA categories including transfer RNA-derived small RNAs (tsRNAs), ribosomal RNA-derived small RNA (rsRNAs), YRNA-derived small RNAs, and piwi-interacting RNA (piRNAs) (21–25). However, the functions of these understudied sncRNAs in atherosclerosis and CVD are mostly unknown. As compared with miRNAs, many of these sncRNAs including tsRNAs and rsRNAs are highly modified since their precursors (e.g., tRNAs and rRNAs) bear various RNA modifications such as RNA methylations (e.g., m⁷G, m¹A, and m³C) (21, 22, 26–28). In addition, terminal modifications (e.g., 3'-phosphate and 2',3'-cyclic phosphate) also commonly occur during tsRNA and rsRNA biogenesis (29–31). These modifications can interfere with the reverse transcription and adaptor ligation processes in the widely used complementary DNA (cDNA) library construction protocol for standard RNA sequencing (RNA-Seq) analysis (22, 29, 32, 33), which prevents the detection of highly modified sncRNAs by the traditional RNA-Seq method (21). To address this issue, we recently developed an innovative RNA-Seq protocol, PANDORA-Seq (Panoramic RNA Display by Overcoming RNA Modification Aborted Sequencing), which employs a combinatorial enzymatic treatment protocol to remove key RNA modifications that block adapter ligation and reverse transcription processes during cDNA library construction (22). PANDORA-Seq has enabled us to detect the highly modified sncRNAs including tsRNAs and rsRNAs, resulting in the discovery of higher abundant levels of tsRNAs/rsRNAs in various tissues and cell types that were undetectable by traditional RNA-Seq (21, 22, 34).

In the current study, we used PANDORA-Seq to identify novel sncRNAs that are associated with atherosclerosis development in LDL receptor-deficient (LDLR^{-/-}) mice. By overcoming RNA modification-elicited limitations, PANDORA-Seq unveiled an rsRNA- and tsRNA-enriched sncRNA landscape in the atherosclerotic intima of LDLR^{-/-} mice, which was strikingly different from that detected by traditional RNA-Seq. We also found that one of the tsRNAs, tsRNA-Arg-CCG, was upregulated in the atherosclerotic intima of LDLR^{-/-} mice. Interestingly, tsRNA-Arg-CCG can affect the expression of proatherogenic genes in human endothelial cells, which may contribute to atherosclerosis development.

MATERIALS AND METHODS

Animals

Three-week-old male LDLR^{-/-} mice on C57BL/6 background (Jackson Laboratories) were fed ad libitum on a semisynthetic low-fat (4.2% fat) AIN76 diet containing either low cholesterol (low-cholesterol diet [LCD]; 0.02% cholesterol; Research Diets) or high cholesterol (high-cholesterol diet [HCD]; 0.5% cholesterol; Research Diets) for 9 weeks until they were euthanized at 12 weeks of age (12, 35–37). All animals

were housed in pathogen-free microisolator cages in a temperature-controlled environment with a 12-h light-dark cycle. All experimental mice used in this study were male. However, studying a single sex has limitations since sex differences have been widely reported in mouse atherosclerosis studies (38). Body composition was measured by EchoMRI (Echo Medical System) (39–41), and intraperitoneal glucose tolerance test was performed as previously described (36, 37). On the day of euthanasia, mice were fasted for 6 h following the dark cycle (feeding cycle), and blood and major organs were collected as previously described (36, 40, 42). All animal studies were performed in compliance with the approved protocols by the Institutional Animal Care and Use Committee of the University of California, Riverside.

Blood analysis

Serum total cholesterol and total triglyceride concentrations were measured using the Wako Cholesterol E enzymatic colorimetric assay (Wako; catalog no.: 999-02601) and the Wako L-type TG M assay (Wako; catalog no.: 994-02891) according to the manufacturer's instructions (FUJIFILM Medical Systems USA, Inc, Richmond, VA). The lipoprotein fractions were isolated in a Beckman Coulter XPN100-IVD ultracentrifuge as previously described (40, 43). Lipoprotein fractions were isolated by centrifuging 60 μ l of serum at 40,000 rpm for 5 h at 4°C in a Beckman Coulter Type 42.2 Ti Rotor at its own density (1.006 g/ml). The infranatant was then adjusted to a density of 1.063 g/ml with solid potassium bromide to harvest the VLDL (<1.006 g/ml), LDL (1.006 \leq d \leq 1.063 g/ml), and HDL (d > 1.063 g/ml) fractions by spinning at 40,000 rpm for 24 h at 4°C. The cholesterol content of the lipoprotein fractions was then measured enzymatically (Wako; cholesterol; catalog no.: 999-02601).

Atherosclerotic lesion analyses

The atherosclerotic lesion sizes were quantified as previously described (9, 12, 44, 45). To quantify the plaque area at the aortic root, OCT-compound-embedded hearts were sectioned at a 12- μ m thickness keeping all the three valves of the aortic root in the same plane and stained with Oil Red O. To quantify atherosclerotic plaque area at the brachiocephalic artery (BCA), the OCT-embedded brachiocephalic arteries were sectioned from distal to proximal at a thickness of 10 μ m. BCA atherosclerotic lesions from the luminal to the internal elastic lamina were quantified in three equidistant Oil Red O-stained sections at 200, 400, and 600 μ m proximal from the branching point of the BCA into the carotid and subclavian arteries. Images were taken, and plaque size was quantified using a Nikon microscope (Nikon, Melville, NY).

Immunohistochemistry

The aortic root of the mice freshly embedded in OCT and sectioned were first fixed in 4% paraformaldehyde for 15 min and permeabilized with 0.1% Triton X-100 in PBS for 15 min. The slides were then blocked with Triton X-100 in PBS containing 5% BSA (Sigma-Aldrich; catalog no.: A9647) for 1 h at room temperature. For immunostaining, slides were incubated with antibodies against CD68 (Bio-Rad AbD Serotec; catalog no.: MCA1957) and alpha smooth muscle actin (Abcam; catalog no.: ab5694) at 4°C for 12–15 h (5, 36, 44). The sections were rinsed with PBS and incubated with fluorescein-labeled secondary antibodies (Life Technologies). The nuclei were stained by mounting the slides with 4',6-diamidino-2-

phenylindole medium (Vector Laboratories). Samples were imaged and analyzed with a Nikon fluorescence microscope. Images were taken, and the positively labeled area was quantified using a Nikon microscope. For trichrome staining, the aortic root freshly embedded in OCT and sectioned were stained with a trichrome stain (Masson) kit (Sigma-Aldrich; catalog no.: HT15) according to the manufacturer's instructions with some modifications to accommodate for frozen tissue (5, 36, 46). Briefly, sections were fixed in 4% paraformaldehyde for 30 min and then stained with Biebrich Scarlet-Acid Fuchsin Solution for 1 min to stain the fibers red. The samples were rinsed with double-distilled H₂O and placed in working phosphotungstic/phosphomolybdic acid solution for 1 h followed directly with Aniline Blue staining for 1 min. Finally, samples were placed in 1% glacial acetic acid for 2 min and mounted with Permount. Images were taken, and collagen content was quantified using Nikon NIS-elements platform (Nikon, Melville, NY).

Cell culture and transfection

Human endothelial cell line HMEC-1 was purchased from ATCC (catalog no.: CRL-3243) (47). HMEC-1 cells passaged less than 20 times were used for transfection. Synthetic control Oligo and tsRNA-Arg-CCG Oligo (Sigma-Aldrich) was transfected into the cells with Lipofectamine RNAiMAX (Thermo Fisher; catalog no.: 13778100) (48) followed by RNA isolation after 24 h. Total RNAs were isolated using TRIzol reagent (Sigma-Aldrich; catalog no.: T9424) as previously described (34, 45).

Northern blot

Northern blot was performed as we previously described (22). Total RNAs isolated from HMEC-1 cells were separated by a 10% urea-PAGE gel followed by SYBR gold staining of nucleic acids (Thermo Fisher; catalog no.: S11494) and immediately imaged. The RNA was then transferred to a positively charged nylon membrane (Roche; catalog no.: 11417240001) and ultraviolet crosslinked with 0.12 J of energy. Membranes were hybridized with PerfectHyb Plus Hybridization Buffer (Sigma-Aldrich; catalog no.: H7033) for 1 h at 42°C. To detect tsRNA-Arg-CCG, membranes were incubated overnight in 42°C with a DIG-labeled oligonucleotide probe (5'-DIG-CGAACCCACAATCCCCAGCT-3').

Intimal RNA isolation

The aortas of LDLR^{-/-} mice were isolated and flushed with PBS followed by intimal peeling using TRIzol reagent (Sigma-Aldrich; catalog no.: T9424) (20). A total of ~300–400 µl of Trizol was flushed through the aorta lumen for 10 s (~100 µl) followed by a 10-s pause and repeated three times, as previously described (20, 49). The flowthrough was collected in a 1.5 ml Eppendorf tube followed by RNA extraction as previously described (22, 40, 42). Total RNAs from the remaining aorta (media and adventitia) were also isolated using TRIzol for gene expression analyses. Intimal RNA integrity and concentrations were confirmed using an Agilent 2100 Bioanalyzer and Aligent RNA 6000 Nano Kit (Agilent Technologies, Inc; catalog no.: 5067-1511) (22).

Quantitative real-time PCR analyses

Quantitative real-time PCR was performed by using gene-specific primers and SYBR Green PCR kit (Bio-Rad

Laboratories) on a Bio-Rad CFX Real-Time-PCR Machine as previously described (12, 34, 40). The sequences of primers used in this study are listed in supplemental Table S8.

PANDORA-Seq of intimal small RNAs

PANDORA-Seq protocol has been recently described in our recent report (22). Here, we provided detailed information for PANDORA-Seq of intimal small RNAs. A schematic of PANDORA-Seq workflow is also included in Figure 1.

Isolation of specified size RNA from total RNAs. The RNA sample from the intima was mixed with an equal volume of 2× RNA loading dye (New England Biolabs; catalog no.: B0363S) and incubated at 75 °C for 5 min. The mixture was loaded into 15% (w/v) urea polyacrylamide gel (10 ml mixture containing 7 M urea [Invitrogen; catalog no.: AM9902]), 3.75 ml acrylamide/Bis 19:1, 40% (Ambion; catalog no.: AM9022), 1 ml 10× TBE (Invitrogen; catalog no.: AM9863), 1 g l⁻¹ ammonium persulfate (Sigma-Aldrich; catalog no.: A3678-25G), and 1 ml l⁻¹ TEMED (Thermo Fisher Scientific; catalog no.: BP150-100) and run in a 1× TBE running buffer at 200 V until the bromophenol blue reached ~1 cm from the bottom of the gel. Small RNA of 15–50 nucleotides was visualized with SYBR Gold solution (Invitrogen; catalog no.: S11494) and excised based on a small RNA ladder (New England Biolabs; catalog no.: N0364S) (22). The RNA was eluted in 0.3 M sodium acetate (Invitrogen; catalog no.: AM9740) and 100 U ml⁻¹ RNase inhibitor (New England Biolabs; catalog no.: M0314L) overnight at 4 °C. The samples were then centrifuged for 10 min at 120,00 g at 4°C. The aqueous phase was mixed with pure ethanol, 3 M sodium acetate, and linear acrylamide (Invitrogen; catalog no.: AM9520) at a ratio of 3:9:0.3:0.01 and incubated at -20 °C for 2 h and centrifuged for 25 min at 12,000 g at 4°C (22). After removing the supernatant, the precipitate was resuspended in nuclease-free water.

Treatment of RNA with AlkB. The intimal RNA was incubated in a 50 µl reaction mixture containing 50 mM Hepes (Fisher Scientific; catalog no.: 15630080), 75 µM ferrous ammonium sulfate, 1 mM α-ketoglutaric acid (Sigma-Aldrich; catalog no.: K1128), 2 mM sodium ascorbate, 50 mg l⁻¹ bovine serum albumin (Sigma-Aldrich; catalog no.: A9647), 4 µg ml⁻¹ AlkB, 2,000 U ml⁻¹ RNase inhibitor, and RNA at 37°C for 30 min (22). Then, the mixture was added into 500 µl TRIzol reagent for RNA isolation.

Treatment of RNA with T4PNK. The intimal RNA was incubated in 50 µl reaction mixture containing 5 µl 10× PNK buffer (New England Biolabs; catalog no.: B0201S), 1 mM ATP (New England Biolabs; catalog no.: P0756S), 10 U T4PNK (New England Biolabs; catalog no.: M0201L), and RNA at 37°C for 20 min (22). Then, the mixture was added into 500 µl TRIzol reagent for RNA isolation.

Small RNA library construction and deep sequencing. The adapters were obtained from the NEBNext Small RNA Library Prep Set for Illumina (New England Biolabs; catalog no.: E7330S) and ligated sequentially. First, we added a 3' adapter system under the following reaction conditions: 70°C for 2 min and 16°C for 18 h. Second, we added a reverse transcription primer under the following reaction conditions: 75°C for 5 min, 37°C for 15 min, and 15°C for 15 min. Third, we added a 5' adapter mix system under the following reaction conditions: 70°C for 2 min and 25°C for 1 h. First-strand

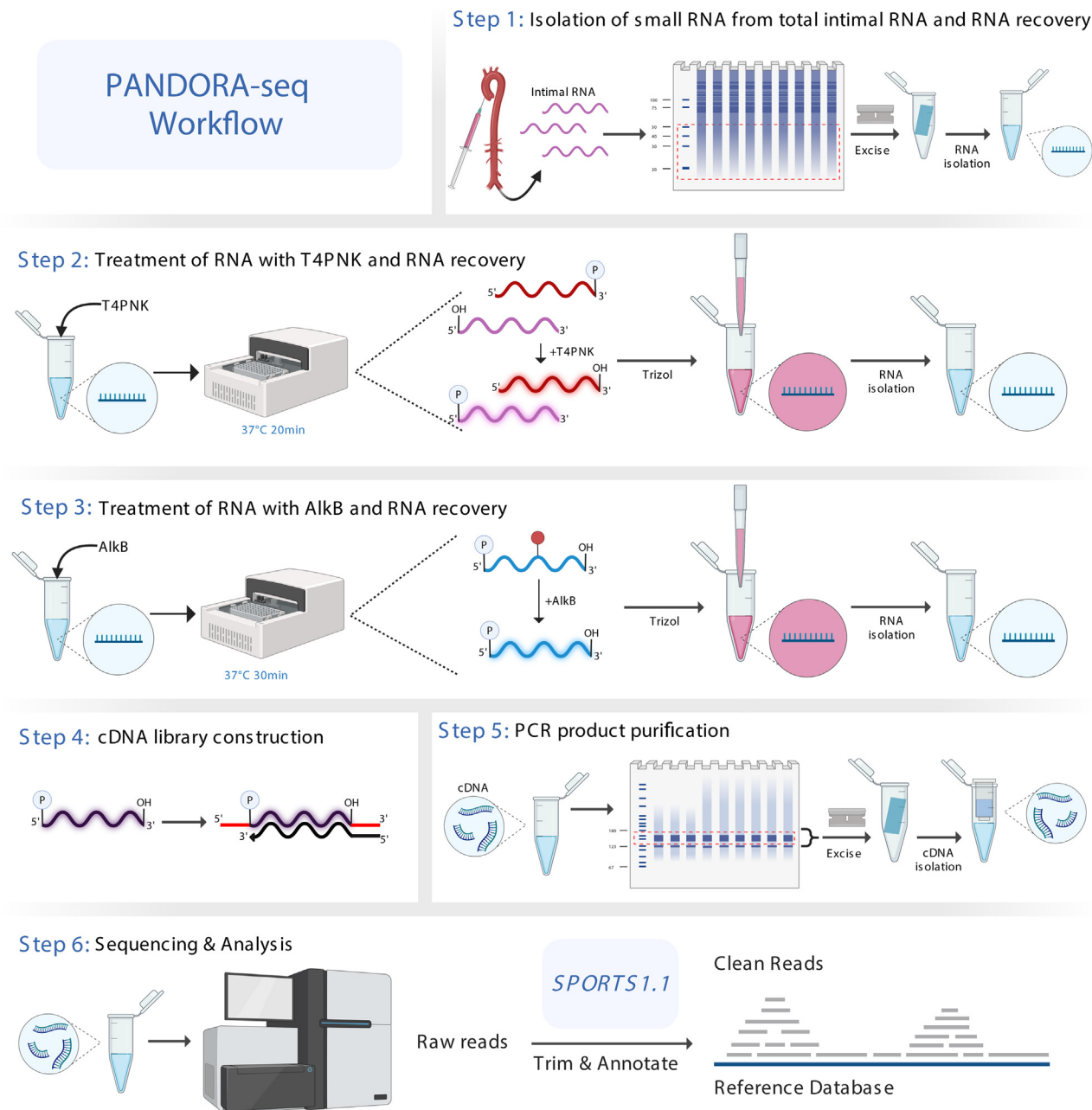


Fig. 1. Schematic of PANDORA-Seq workflow. Step 1: Small RNAs from intimal total RNAs were excised from PAGE gel. Step 2: Purified small RNAs were subjected to T4PNK treatment. Step 3: Purified small RNAs were subjected to Alkb treatment. Step 4: NEBNext Small RNA Library Prep Set for Illumina was used for cDNA library construction. Step 5: PCR products were purified with PAGE gel. Step 6: Final product was sequenced and annotated using the *SPORTS1.1* pipeline. A detailed protocol of PANDORA-Seq is included in the [Materials and Methods](#) section. Image was created by using [BioRender.com](#).

cDNA synthesis was performed under the following reaction conditions: 70°C for 2 min and 50°C for 1 h. PCR amplification with PCR Primer Cocktail and PCR Master Mix was performed to enrich the cDNA fragments under the following conditions: 94°C for 30 s; 17 cycles of 94°C for 15 s, 62°C for 30 s, and 70°C for 15 s; 70°C for 5 min; and hold at 4°C. Then, the PCR product was purified from PAGE gel.

Small RNA annotation and analyses for PANDORA-Seq data.-

Small RNA sequences were annotated using the software sRNA annotation pipeline optimized for rRNA- and tRNA-derived sRNAs (SPORTS) 1.1 (56) with one mismatch tolerance

(SPORTS1.1 parameter setting: -M 1). Reads were mapped to the following individual ncRNA databases sequentially: (1) the miRNA database miRBase 21; (2) the genomic tRNA database GtRNAdb; (3) the mitochondrial tRNA database mitotRNAdb; (4) the rRNA and YRNA databases assembled from the National Center for Biotechnology Information nucleotide and gene database; (5) the piRNA databases, including piRBase and piRNABank; and (6) the ncRNAs defined by Ensembl and Rfam 12.3. The tsRNAs were annotated based on both pre-tRNA and mature tRNA sequences. Mature tRNA sequences were derived from the GtRNAdb and mitotRNAdb sequences using the following procedures: (1) predicted introns were removed; (2) a CCA sequence was added to the 3'

ends of all tRNAs; and (3) a G nucleotide was added to the 5' ends of histidine tRNAs. The tsRNAs were categorized into four types based on the origin of the tRNA loci: 5' tsRNA (derived from the 5' end of pre-tRNA/mature tRNA); 3' tsRNA (derived from the 3' end of pre-tRNA); 3' tsRNA-CCA end (derived from the 3' end of mature tRNA); and internal tsRNAs (not derived from 3' or 5' loci of tRNA). For the rsRNA annotation, we mapped the small RNAs to the parent rRNAs in an ascending order of rRNA sequence length to ensure a unique annotation of each rsRNA (e.g., the rsRNAs mapped to 5.8S rRNA would not be further mapped to the genomic region overlapped by 5.8S and 45S rRNAs). We then employed the *edgeR* algorithm (50) to perform the comparison of sncRNA expression patterns between groups. We applied the *TMM* algorithm to perform read count normalization and effective library size estimation and the likelihood ratio test to identify the differentially expressed sncRNA species. The sncRNA species with a false discovery rate (FDR) <0.1 and fold change (FC) >2 were deemed differentially expressed.

Intimal transcriptome analysis

The creation of cDNA libraries and sequencing were performed using the Illumina standard operation pipeline as previously described (36, 42, 45, 51, 52). For data analysis, we applied the *Salmon* tool to quantify the mRNA expression from the raw sequencing data with the default setting, based on the Ensembl mouse cDNA annotation (GRCm38). We then employed the *edgeR* algorithm (50) to perform the comparison in transcriptomic pattern between groups, using the *TMM* algorithm to perform read count normalization and effective library size estimation and the likelihood ratio test to identify the differentially expressed genes (DEGs). The genes with FDR <0.1 and FC >2 were deemed differentially expressed. We further performed pathway analysis upon the DEGs using the definition from Kyoto Encyclopedia of Genes and Genomes (KEGG) project. For each KEGG pathway, we computed a geneset score, using the Functional Analysis of Individual Microarray Expression (FAIME) algorithm (53). A higher FAIME score suggests a higher overall expression of a given pathway. All the RNA-Seq datasets have been deposited in the Gene Expression Omnibus (GSE213305).

Statistical analysis

All data except the high-throughput sequencing data are presented as the mean \pm SEM. Individual pairwise comparisons were analyzed by two-sample, two-tailed Student's *t*-test unless otherwise noted, with *P* < 0.05 regarded as significant using GraphPad Prism (GraphPad Software, Inc). One-way ANOVA with uncorrected Fisher's least significant difference test was used for analyzing different origins of the tsRNA/miRNA expression ratio under different treatments. N numbers are listed in figure legends.

RESULTS

Feeding LDLR^{-/-} mice a low-fat HCD promotes hypercholesterolemia without affecting adiposity and metabolic phenotypes

To investigate sncRNAs associated with atherosclerosis development, male LDLR^{-/-} mice were fed a low-fat (4.3% fat) AIN76 diet containing 0.02% or 0.5% cholesterol for 9 weeks (35). We and others have

successfully used this diet to induce atherosclerosis development without eliciting obesity and associated metabolic disorders in LDLR^{-/-} or ApoE^{-/-} mice (35–37, 45, 54, 55). Consistently, we found that LDLR^{-/-} mice fed the relatively HCD (0.5% cholesterol) had similar body weight and growth curve as mice fed the LCD (0.02% cholesterol) (Fig. 2A). HCD- and LCD-fed mice also had similar body composition, including fat mass and lean mass (Fig. 2B). Glucose tolerance tests also demonstrated that exposure to these diets did not alter glucose tolerance in LDLR^{-/-} mice (Fig. 2C). Consistent with previous results (35, 54), HCD feeding led to elevated serum total cholesterol levels without affecting triglyceride levels (Fig. 2D). Lipoprotein fraction analysis was then performed, and mice fed HCD had significantly higher atherogenic LDL and VLDL cholesterol levels but similar HDL cholesterol levels as compared with LCD-fed mice (Fig. 2E). Thus, the low-fat HCD can promote hypercholesterolemia without inducing obesity or metabolic disorders in LDLR^{-/-} mice.

HCD feeding effectively induces atherosclerosis development in lean LDLR^{-/-} mice

Atherosclerotic lesion areas were then analyzed in the aortic root and BCA of LCD- or HCD-fed LDLR^{-/-} mice. We found that HCD feeding significantly increased atherosclerotic lesion areas in the aortic root of LDLR^{-/-} mice as compared with LCD-fed mice (183,487.7 \pm 48,193.4 μm^2 vs. 8,378.9 \pm 4,142.7 μm^2) (Fig. 2F). Short-term LCD feeding did not induce observable atherosclerosis development in BCA of LDLR^{-/-} mice (Fig. 2G). However, exposure to HCD significantly increased the atherosclerotic lesion areas in the BCA of LDLR^{-/-} mice (8,559.8 \pm 3,652.6 μm^2 vs. 0 \pm 0 μm^2) (Fig. 2G).

In addition to lesion size, we characterized multiple factors that are associated with atherosclerosis development, including macrophage infiltration, SMC migration, and collagen production. As expected, immunostaining for macrophage and SMC markers showed increased macrophage contents and SMC migration in the atherosclerotic plaque of HCD-fed LDLR^{-/-} mice (supplemental Fig. S1, A–C). Furthermore, Masson's Trichrome staining also demonstrated that HCD feeding led to increased collagen content in the atherosclerotic lesions of LDLR^{-/-} mice as compared with LCD-fed mice (supplemental Fig. S1D). Collectively, these results demonstrate that the low-fat HCD feeding can effectively induce atherosclerosis development in lean LDLR^{-/-} mice.

Transcriptome analysis reveals altered atherosclerosis-related gene expression in the intima of HCD-fed LDLR^{-/-} mice

We next isolated intimal RNAs for regular RNA-Seq analysis to understand the transcriptomic changes in the intima of LDLR^{-/-} mice. Total RNAs isolated from the intima and remaining aortic fraction were first

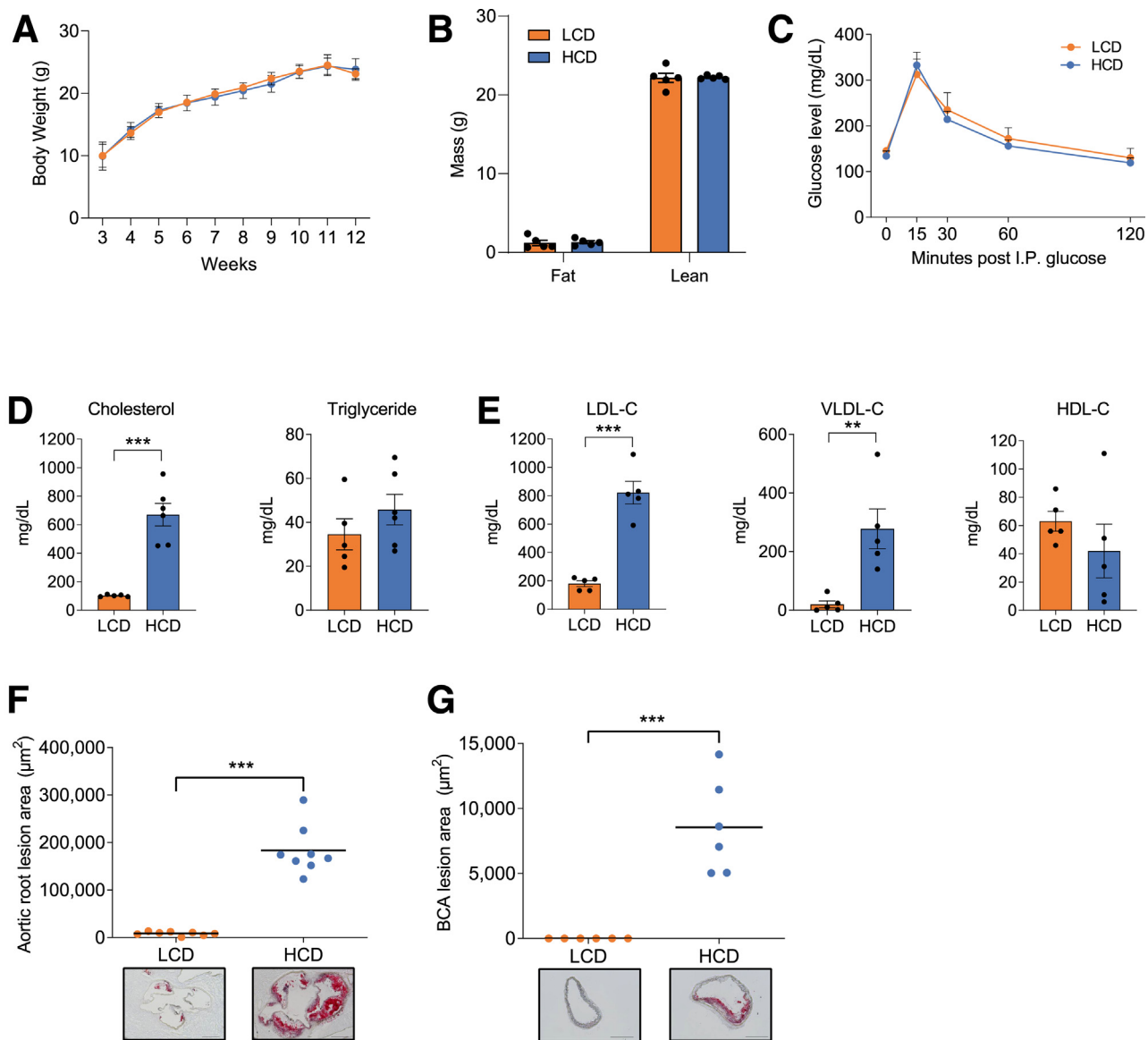


Fig. 2. A low-fat HCD effectively promotes hypercholesterolemia and atherosclerosis without inducing obesity and insulin resistance in LDL receptor-deficient mice. Three-week-old male $LDLR^{-/-}$ mice were fed an LCD (0.02% cholesterol) or HCD (0.5% cholesterol) for 9 weeks until euthanasia at 12 weeks of age. (A–C) Growth curves (A), body composition (B), and intraperitoneal glucose tolerance test (C) of LCD- and HCD-fed $LDLR^{-/-}$ mice. (D) Serum total cholesterol and triglyceride levels were measured. (E) Lipoprotein fractions (VLDL-C, LDL-C, and HDL-C) were isolated, and the cholesterol levels of each fraction were measured. (F) Quantitative analysis of the lesion area in the aortic root. Representative Oil Red O-stained aortic root sections displayed below the quantification data (scale bar represents 200 μm). (G) Quantitative analysis of the lesion area in the BCA. Representative Oil Red O-stained BCA sections displayed below quantification data (scale bar represents 200 μm). All data are plotted as means \pm SEM ($n = 5\text{--}8$ each group; $*P < 0.05$; $**P < 0.01$; $***P < 0.001$).

characterized for endothelial marker (e.g., *VE-Cadherin* and *Tie2*) and SMC marker (*Myh11* and α -Smooth muscle actin) expression. Consistent with previous studies (20), our results confirmed the enrichment of endothelial cell markers and the low expression levels of SMC markers in the intima as compared with that of media/adventitia (supplemental Fig. S2). By contrast, the media/adventitial fraction has high expression levels of SMC markers but low expression levels of endothelial cell markers (supplemental Fig. S2).

RNA-Seq analysis of the intima uncovered 1,313 DEGs in the intima of HCD-fed $LDLR^{-/-}$ mice as

compared with LCD-fed mice with an FDR of <0.1 and FC >2 as the cutoff threshold (Fig. 3A and supplemental Table S1). KEGG analysis then revealed that many upregulated DEGs were enriched in several biological processes that contribute to atherosclerosis development including “cytokine-cytokine receptor interaction,” “chemokine signaling pathway,” and “cell adhesion molecules” (Fig. 3B). In addition, some DEGs were also enriched in lysosome- and phagosome-associated pathways that are also important for atherosclerosis development (Fig. 3B). By using the FAIME algorithm, we verified that the geneset scores of

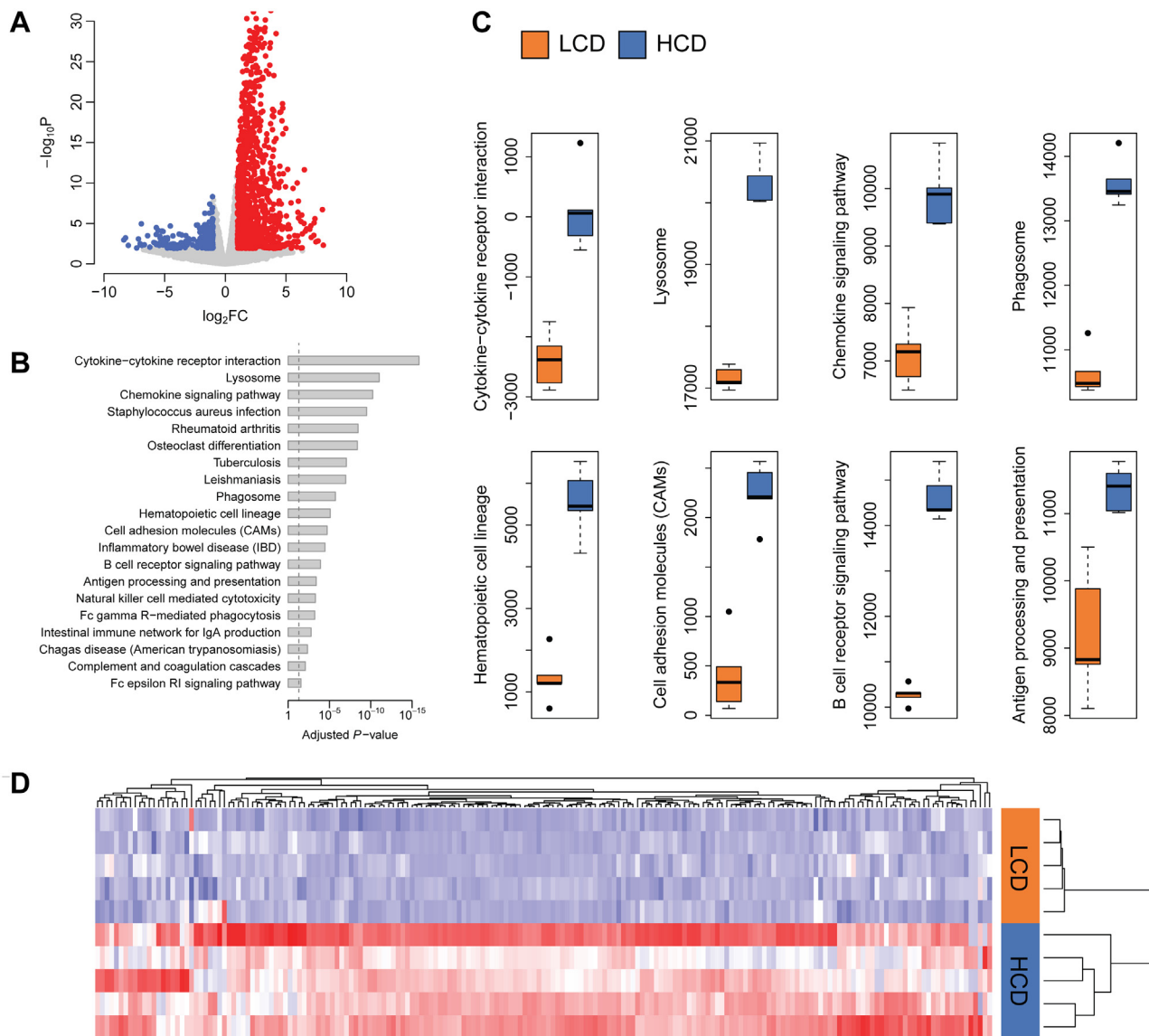


Figure 3. HCD feeding affects many atherosclerosis-related gene expression in the intima of LDL receptor-deficient mice. Three-week-old male $LDLR^{-/-}$ mice were fed an LCD or HCD for 9 weeks. Total RNA was isolated from the intima and used for RNA-Seq analysis. (A) Volcano plot of DEGs in the intima of HCD-fed $LDLR^{-/-}$ mice as compared with LCD-fed mice. Colored dots represent the enriched (red dots) or depleted (blue dots) DEGs with an FDR of <0.1 and FC >2 as a cutoff threshold. (B) KEGG pathways significantly associated with upregulated DEGs in intimal of HCD-fed $LDLR^{-/-}$ mice. The P values were computed by Fisher's exact test. The vertical dash line indicates the significance level of $\alpha = 0.05$. The y-axis displays the KEGG pathways, whereas the x-axis displays the adjusted P -values. (C) Geneset scores of the prioritized KEGG pathways. The geneset score was calculated using the FAIME algorithm. (D) Heatmap representation of DEGs involved in the pathways of "cytokine-cytokine receptor interaction," "chemokine signaling pathway," and "cell adhesion molecules," "lysosome," "phagosome", "hematopoietic cell lineage," "B-cell receptor signaling pathway," and "antigen processing and presentation." Each column shows one individual gene, and each row shows a biological replicate of mouse. Red represents relatively increased gene expression, whereas blue denotes downregulation ($n = 5$ each group).

these pathways were significantly increased in HCD-fed $LDLR^{-/-}$ mice as compared with LCD-fed mice (Fig. 3C). The genes associated with these pathways were also upregulated in HCD-fed $LDLR^{-/-}$ mice (Fig. 3D). Taken together, intimal RNA-Seq analysis confirmed the altered atherosclerosis-related genes and pathways that are associated with the increased atherosclerosis in HCD-fed $LDLR^{-/-}$ mice.

PANDORA-Seq but not traditional RNA-Seq unveils an rsRNA- and tsRNA-enriched snRNA landscape in the atherosclerotic intima of $LDLR^{-/-}$ mice

Many snRNAs bear specific modifications, which can prevent the detection of snRNAs in widely used traditional RNA-Seq methods (21). To overcome this obstacle, we recently developed a novel small RNA-Seq method, PANDORA-Seq, to eliminate the RNA

modification-elicited sequence interferences (Fig. 1) (22). To determine whether PANDORA-Seq can detect novel sncRNAs associated with atherosclerosis development, intimal RNA was collected and processed through both traditional small RNA-Seq and PANDORA-Seq followed by SPORTS1.1 bioinformatics analysis (22, 56). Since miRNAs are not as highly modified as other sncRNAs such as rsRNAs/tsRNAs, they can be readily detected by traditional sequencing (21, 22). Indeed, traditional sequencing detected an miRNA-enriched sncRNA landscape in the intima of

both LCD- (47.9%) and HCD (55.9%)-fed $LDLR^{-/-}$ mice (Fig. 4A). However, PANDORA-Seq revealed a totally different sncRNA landscape in which rsRNAs and tsRNAs account for 83.1% (LCD) and 82.4% (HCD) of total detected sncRNAs in the intima of $LDLR^{-/-}$ mice (Fig. 4A).

As rsRNA reads were dominant in PANDORA-Seq results, which consumed the relative reads of other sncRNAs (Fig. 4A), we filtered out rsRNAs from the total sncRNA reads and found that PANDORA-Seq but not traditional RNA-Seq detected an increased

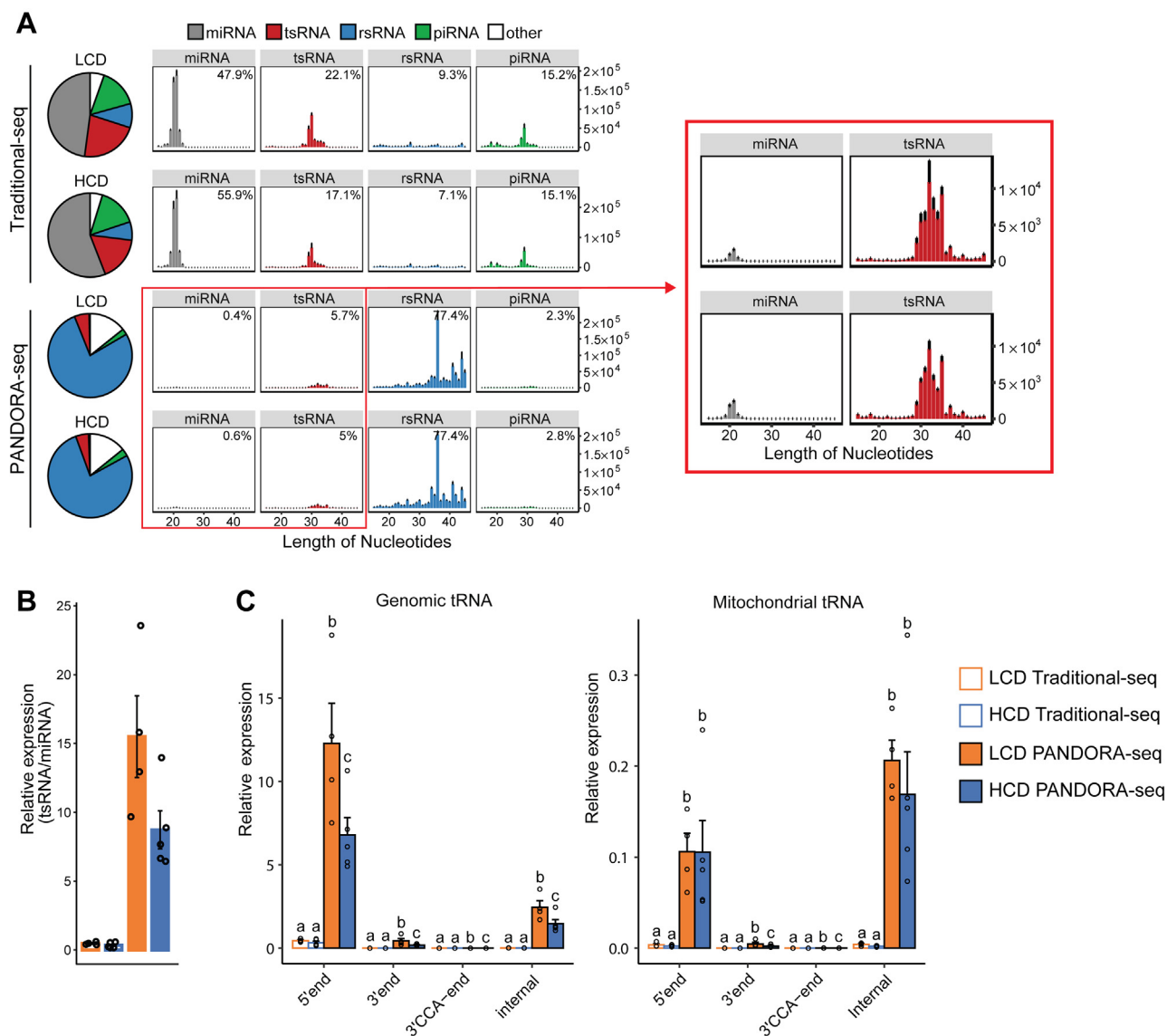


Fig. 4. Read summaries and length distributions of different sncRNA categories in the intima of LDL receptor-deficient mice under traditional RNA-Seq and PANDORA-Seq. Three-week-old male $LDLR^{-/-}$ mice were fed an LCD or HCD for 9 weeks. Total RNA was isolated from the intima and used for PANDORA-Seq or traditional small RNA sequencing. (A) Dynamic landscapes of intimal sncRNAs including miRNAs, tsRNAs, rsRNAs, and piRNAs detected by traditional-Seq and PANDORA-Seq protocols. Zoomed panels of miRNAs and tsRNAs detected by PANDORA-Seq are shown on the right. (B) Relative tsRNA/miRNA ratios under traditional-Seq and PANDORA-Seq protocols. (C) tsRNA responses to traditional-Seq and PANDORA-Seq with regard to different origins (5' tsRNA, 3' tsRNA, 3' tsRNA-CCA end, and internal tsRNAs). The y-axes represent the relative expression levels compared with total reads of miRNA. Different letters above the bars indicate statistically significant differences ($P < 0.05$). Same letters indicate $P > 0.05$. Statistical significance was determined by two-sided one-way ANOVA with uncorrected Fisher's least significant difference test. All data are plotted as means \pm SEM ($n = 4-5$ in each group).

tsRNA:miRNA ratio in both LCD- and HCD-fed mice (Fig. 4B). The origins, from which the tsRNAs are derived (5'tsRNAs, 3'tsRNAs, 3'tsRNAs with a CCA end, and internal tsRNAs), were also analyzed. PANDORA-Seq revealed an increased relative expression of specific tsRNA origins as compared with traditional RNA-Seq (Fig. 4C). Consistent with previous studies, a majority of tsRNAs are derived from the 5' end of mature tRNAs (22). Specific rRNA loci, where rsRNA are derived, were also evaluated, and the data demonstrate increased rsRNA detection by PANDORA-Seq (supplemental Fig. S3). These results suggest that PANDORA-Seq can detect highly modified sncRNAs such as tsRNAs and rsRNAs in the atherosclerotic intima of LDLR^{-/-} mice that were otherwise undetectable by the traditional RNA-Seq method.

PANDORA-Seq detects more differentially expressed sncRNAs associated with atherosclerosis development in the intima of HCD-fed LDLR^{-/-} mice

We further analyzed both PANDORA-Seq and traditional RNA-Seq results to determine how HCD feeding alters the expression levels of sncRNAs in the intima of LDLR^{-/-} mice. While traditional RNA-Seq only detected a small number of differentially regulated sncRNAs, including only 16 rsRNAs and tsRNAs, PANDORA-Seq detected a total of 1,383 differentially regulated sncRNAs (FC >2 and FDR <0.1), including 1160 rsRNAs and 195 tsRNAs (Fig. 5A and supplemental Tables S2–S7). PANDORA-Seq also detected 28 differentially regulated miRNAs in the intima of HCD-fed LDLR^{-/-} mice (Fig. 5B and supplemental Table S4).

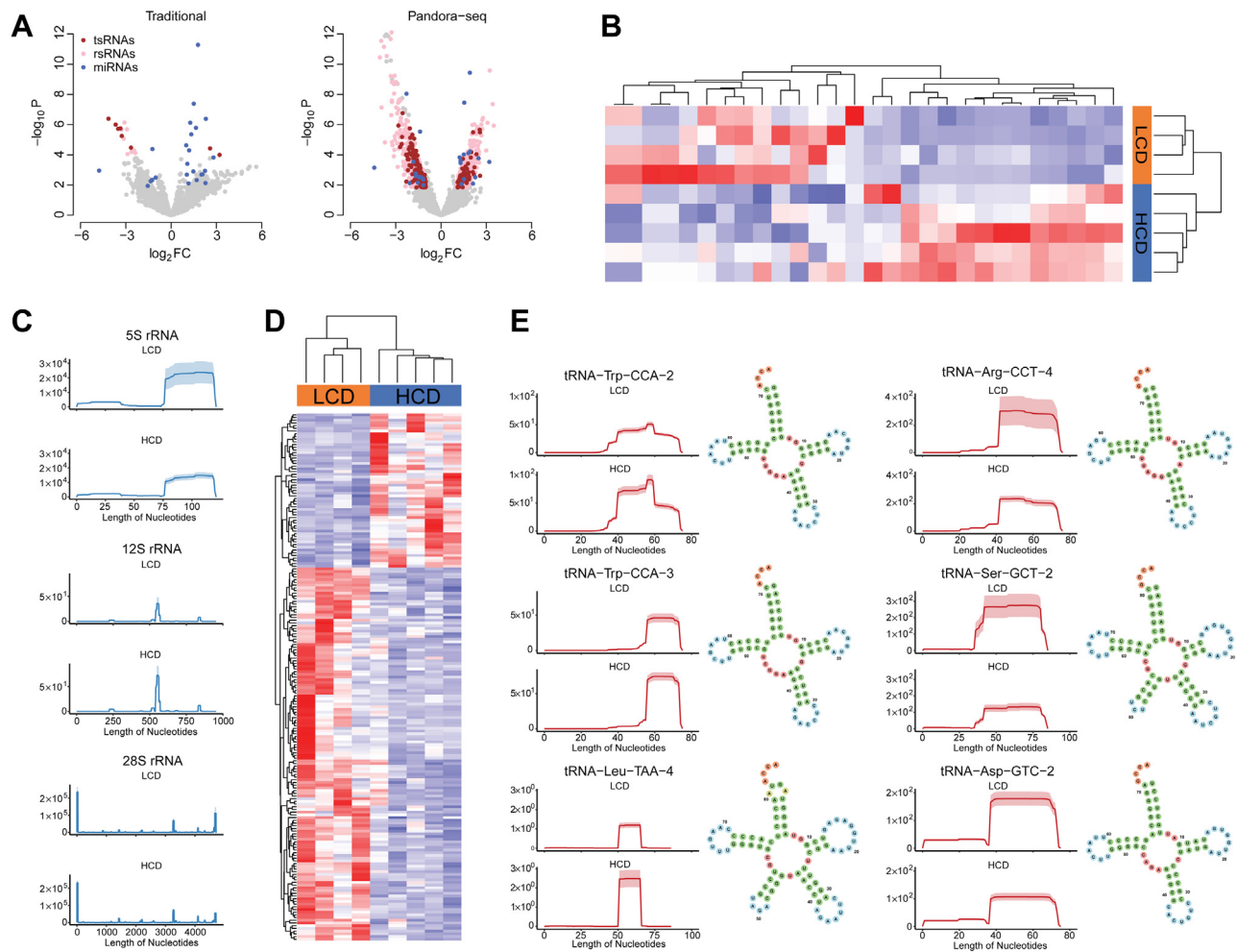


Fig. 5. Identification of significantly altered intimal sncRNAs associated with atherosclerosis development in LDL receptor-deficient mice by PANDORA-Seq and traditional RNA-Seq. Three-week-old male LDLR^{-/-} mice were fed an LCD or HCD for 9 weeks. Total RNA was isolated from the intima and used for PANDORA-Seq or traditional small RNA-Seq. (A) Volcano plot of differentially expressed intimal sncRNAs identified by traditional sequencing (left) and PANDORA-Seq methods (right). Colored dots represent the differentially expressed tsRNAs (red dots), rsRNAs (pink dots), or miRNAs (blue dots) with an FDR <0.1 and FC >2 as the cutoff threshold. (B) Heatmap representation of differentially expressed intimal miRNAs detected by PANDORA-Seq. (C) Comparison of rsRNA-generating loci by rsRNA mapping data on 5S rRNA, 12S rRNA, and 28S rRNA detected by PANDORA-Seq. (D) Heatmap representation of differentially expressed intimal tsRNAs detected by PANDORA-Seq. (E) Dynamic responses to LCD or HCD of representative individual tsRNAs (pictured right). Biological replicates are represented in each row (B) or column (D). Red represents relatively increased expression, whereas blue represents decreased expression with an FDR <0.1 and FC >2 as the cutoff threshold ($n = 4-5$ each group).

Many of those miRNAs are consistent with previous reports such as miR-146b, miR-155, and miR-125a, though the functions of these miRNAs on atherogenesis have not been completely understood (17, 18).

Next, we compared rsRNA expression patterns between LCD- and HCD-fed LDLR^{-/-} mice from individual ribosomal RNA (e.g., 5S, 12S, and 28S) by analyzing the specific loci where rsRNAs were derived (Figs. 5C and S3). The mapping of rsRNAs from 5S, 12S, and 28S, used as examples, showed dynamic expression patterns in response to HCD feeding detected by PANDORA-Seq (Fig. 5C). We also generated a heatmap to compare the 195 significantly altered intimal tsRNAs between HCD- and LCD-fed mice detected by PANDORA-Seq (Fig. 5D and supplemental Table S2). Furthermore, mapping of tsRNA expression patterns on individual tRNA length scales (tRNA-Trp, tRNA-Arg, tRNA-Ser, tRNA-Leu, and tRNA-Asp used as examples) revealed that those tsRNAs also contain distinct dynamic responses to HCD feeding (Fig. 5E). The functions of those tsRNAs are mostly unknown, and more studies are required to investigate the role of those tsRNAs in atherogenesis.

HCD-induced tsRNA-Arg-CCG affects proatherogenic gene expression in endothelial cells in vitro

Endothelial cells play an essential role in regulating vascular inflammation and the initiation and

progression of atherosclerosis (7). To investigate the potential function of tsRNAs identified by PANDORA-Seq in atherosclerosis, we selected one of the HCD-induced tsRNAs, tsRNA-Arg-CCG, for in vitro analysis. tsRNA precursors, tRNAs, are a highly conserved RNA species (57), and human and murine tRNA-Arg-CCG also shared the same sequence (Fig. 6A). We transfected synthetic tsRNA-Arg-CCG oligonucleotides into human endothelial cells, HMEC-1 cells (47). Northern blot was then performed to confirm the successful overexpression of tsRNA-Arg-CCG in HMEC-1 cells (Fig. 6B). Interestingly, we found that overexpression of synthetic tsRNA-Arg-CCG led to increased expression of several proatherogenic genes, including IL-6, IL-1 α , ICAM-1, VCAM-1, and MCP-1 in HMEC-1 cells (Fig. 6C). Therefore, tsRNA-Arg-CCG may have proatherogenic properties in vivo, which warrants further investigation.

DISCUSSION

sncRNAs are a major family of ncRNAs that play critical roles in numerous biological processes. Certain small RNA populations such as miRNAs and piRNAs have been extensively studied and have also been implicated in atherosclerosis (58, 59). In addition to those well-characterized sncRNAs, recent studies have revealed the wide existence and unexpected functions of new classes of sncRNAs including tsRNAs and

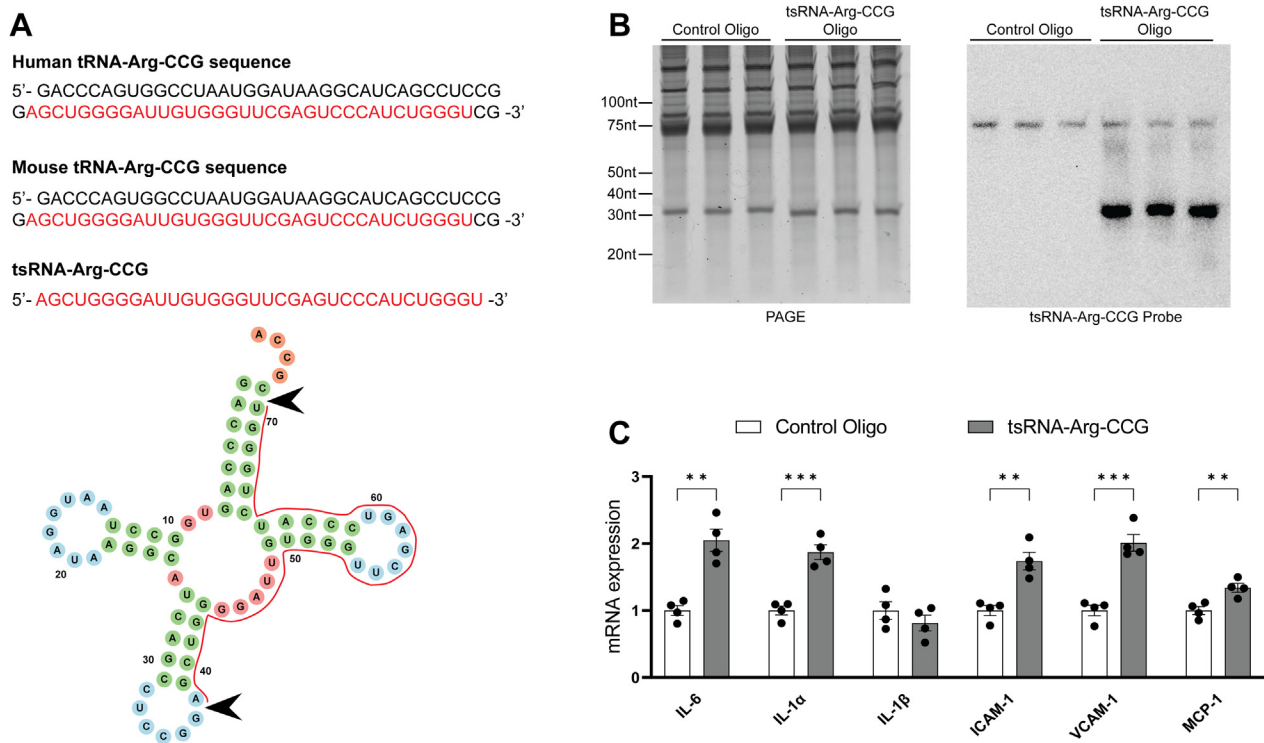


Fig. 6. tsRNA-Arg-CCG affects proatherogenic gene expression in human endothelial cells in vitro. (A) Sequences of human and murine tRNA-Arg-CCG and tsRNA-Arg-CCG (top) and representative figure of tRNA-Arg and tsRNA-Arg-CCG indicated with a red line (bottom; black arrowheads indicating cleavage site). (B and C) Human endothelial cells, HMEC-1 cells, were transfected with synthetic tsRNA-Arg-CCG oligo. The expression levels of tsRNA-Arg-CCG after transfection were assessed with Northern blot (B). Expression levels of indicated genes were analyzed by quantitative real-time PCR (C) ($n = 4$; $**P < 0.01$; $***P < 0.001$).

rsRNAs (28, 56, 60, 61). However, the functions of those noncanonical sncRNAs in atherosclerosis or CVD are mostly unknown. A major obstacle in discovering and studying these sncRNAs is that the currently widely used RNA-Seq protocol generates biased sequencing results and often fails to detect these species (21, 22). Many sncRNAs including tsRNAs and rsRNAs bear RNA modifications that interfere with adapter ligation and reverse transcription processes during cDNA library construction process, leading to unsuccessful detection of tsRNAs and rsRNAs in various tissues and cells (21, 22). For example, tsRNAs contain N¹-methyladenosine (m¹A), N³-methylcytidine (m³C), and N¹-methylguanosine (m¹G) modifications that hinder reverse transcription process during traditional cDNA construction (22, 62). In addition, some sncRNA species, including tsRNAs and rsRNAs, contain 3' terminal modifications such as 5'-phosphate and 2'3'-cyclic phosphate that block adaptor ligation and escape traditional library construction (63). Therefore, the modified tsRNAs, rsRNAs, and other sncRNAs may escape library construction and remain undetected by traditional RNA-Seq. To overcome this obstacle, we recently developed PANDORA-Seq based on a combination of enzymatic treatments (e.g., T4PNK and AlkB treatments) with optimized protocols that improve both RNA 3' and 5' adapter ligation and reverse transcription during cDNA library construction (22). PANDORA-Seq has major advantages over previous methods designed to target either adapter ligation or reverse transcription processes alone, leading to the identification of abundant modified tsRNAs and rsRNAs in various tissues and cells (21, 22, 34). In the current study, PANDORA-Seq unveiled an rsRNA- and tsRNA-enriched sncRNA landscape in the atherosclerotic intima of LDLR^{-/-} mice, which was strikingly different from that detected by traditional RNA-Seq. While miRNAs were the dominant sncRNAs detected by traditional RNA-Seq (e.g., ~56% of total sncRNAs in HCD-fed mice), PANDORA-Seq detected a substantially different sncRNA population with rsRNAs and tsRNAs accounting for >82% of total sncRNAs. In addition, traditional RNA-Seq only detected a few differentially expressed rsRNAs and tsRNAs induced by HCD feeding, but PANDORA-Seq detected more than 1,300 differentially expressed rsRNAs and tsRNAs. Thus, by overcoming RNA modification-elicited limitations, PANDORA-Seq revealed the hidden rsRNA and tsRNA population associated with atherosclerosis development undetected by traditional RNA-Seq.

To identify novel sncRNAs associated with atherosclerosis development, we fed LDLR^{-/-} mice a low-fat LCD or HCD for 9 weeks. As expected, HCD feeding resulted in severe hypercholesterolemia and large atherosclerotic lesions in LDLR^{-/-} mice. The atherosclerotic lesions of LCD-fed mice were quite small, partially because of the relatively short feeding period (9 weeks) and young age of the mice (12 weeks old) at

the time of euthanasia. Previous studies using the same LCD but longer feeding period resulted in larger atherosclerotic lesions (35, 45). However, the relatively big difference of atherosclerotic lesion sizes between LCD- and HCD-fed mice is ideal for the current study. Aiming to identify genes and sncRNAs associated with atherosclerosis development, we also focused on the intima of hypercholesterolemic LDLR^{-/-} mice and performed transcriptome and sncRNA analyses via high-throughput RNA-Seq and PANDORA-Seq. Previous studies have used whole aortic tissues for traditional RNA-Seq (64–67). Since intima is the main site for atherosclerotic plaque initiation and development, we chose to isolate RNAs from the intima for further analyses. As expected, transcriptomic analysis revealed enriched pathways for inflammatory and immune responses, which is consistent with previous studies on whole atherosclerotic arteries and the well-established role of the immune response in atherosclerosis (4, 64, 68). For example, the C-C motif chemokine ligand family (*Ccl2*, *Ccl3*, *Ccl4*, and *Ccl5*) associated with increased inflammatory responses in atherosclerosis (69) was upregulated in the intima of HCD-fed LDLR^{-/-} mice. Our transcriptomic results are consistent with known functions of the genes and pathways in atherogenesis based on the previous human and rodent studies (64, 65, 70–72), which validated our experimental approach using intimal samples.

Previous sncRNA studies in the atherosclerosis research field have mainly focused on the function of miRNAs (16–18). Our PANDORA-Seq results also revealed differentially expressed miRNAs that are consistent with traditional-Seq results and previous reports. For example, miRNA-146, which targets the 3'UTR region of TRAF6 to regulate NF-κB activation, has been shown to be associated with atherosclerosis development or CVD in humans (73, 74). Consistently, we found that miRNA-146b was upregulated in the intima of HCD-fed LDLR^{-/-} mice as compared with LCD-fed mice. In addition, we also found that miRNA-31 was upregulated in atherosclerotic intima of HCD-fed LDLR^{-/-} mice. miRNA-31 is expressed in both endothelial cells (75) and macrophages (76), which targets the 3'UTR region of adhesion molecule E-selection and may also contribute to atherosclerosis development (75–77).

Since miRNAs are not as highly modified as other sncRNAs, such as rsRNAs or tsRNAs (21, 22), miRNAs can be readily detected by traditional-Seq and becomes the major small RNA species in traditional-Seq results. However, these results are misleading as traditional-Seq failed to detect sncRNAs with extensive terminal/internal modifications (21, 22). We have recently comprehensively compared the strengths of PANDORA-Seq to that of traditional-Seq (21, 22) and demonstrated the advantages of PANDORA-Seq enabled by overcoming RNA modifications, which generate sequencing bias in the traditional-Seq method.

In addition to miRNAs, PANDORA-Seq can detect other highly modified rsRNAs and tsRNAs, which were not detected by traditional-Seq (21, 22). Our PANDORA-Seq results showed that percentage of miRNA reads is very small (~0.4–0.6%), but rsRNAs and tsRNAs are much more abundant as compared with miRNA reads, which is consistent with our recent studies (22, 34). However, these results do not mean that PANDORA-Seq failed to detect miRNAs but rather more objectively represent the true compositions of sncRNA population in the intima.


As compared with miRNAs, little is known about the function of tsRNAs and rsRNAs in CVD or atherosclerosis (16). These noncanonical sncRNAs have distinguishable features on evolutionary origin, abundance, biogenesis, and functions (21). Recent studies started to reveal the wide existence and functions of these new classes of sncRNAs (21, 28, 60, 61, 78). For example, tsRNAs are among the most ancient small RNAs in a wide range of species across all domains of life (57) and have received much attention because of their evolutionary conserved sequence and their roles in fundamental biological processes (57, 78–80). The functions of tsRNAs in other disease models, including cancer and metabolic disease, have been described (57, 81–84). However, the role of the tsRNAs in atherosclerosis or CVD is mostly unknown. In the current study, PANDORA-Seq but not traditional-Seq identified many tsRNAs affected by HCD feeding in the intima of LDLR^{-/-} mice. We found that one of HCD-induced intimal tsRNAs, tsRNA-Arg-CCG, may play a role in regulating proatherogenic gene expression in endothelial cells in vitro. It is also important to note that tsRNA modifications can affect their secondary structure and function (21, 82, 83, 85). Although we demonstrated the proatherogenic properties of synthetic unmodified tsRNA-Arg-CCG in vitro, endogenous tsRNA-Arg-CCG with modifications may exert stronger or different phenotypes in vivo. Future studies are required to understand the functions of those tsRNAs in endothelial cell function and atherosclerosis and CVD.

As a low-input and high-throughput method, PANDORA-Seq allows us to detect a vast amount of small RNAs from a low amount of RNA input from the intima. Nevertheless, a potential limitation of PANDORA-Seq is the loss of RNA products during multiple RNA purification steps, which make it difficult to reach the level of single-cell library preparation. To address this limitation in the future, one potential solution is to improve the enzymes used in PANDORA-Seq, which allows the library construction process to be performed in a one-pot reaction, thereby reducing the number of RNA purification steps and minimizing RNA loss. Combining the improved PANDORA-Seq method with fluorescence-activated cell sorting would enable investigators to perform single-cell analysis for detecting cell type-specific highly modified sncRNAs. Future studies using single-cell PANDORA-Seq would

increase our understanding of the cell type-specific role of understudied sncRNAs in atherosclerosis.

In summary, we used a novel PANDORA-Seq to identify sncRNAs associated with atherosclerosis development in LDLR^{-/-} mice. By overcoming RNA modification-elicited limitations, PANDORA-Seq substantially increased the reads of rsRNAs and tsRNAs and revealed an rsRNA- and tsRNA-enriched sncRNA landscape in the atherosclerotic intima of LDLR^{-/-} mice. We also found that one of HCD-induced intimal tsRNA-Arg-CCG has proatherogenic properties and may contribute to endothelial cell dysfunction and atherosclerosis development. To our knowledge, this is the first study to utilize PANDORA-Seq to investigate sncRNAs in atherosclerosis or CVD. Our results suggest that the understudied rsRNAs and tsRNAs are much more abundant than miRNAs in atherosclerosis-prone tissues. Findings from our studies will hopefully stimulate further investigations of the functions of these previously underexplored sncRNAs in atherosclerosis or CVD.

Data availability

The RNA-Seq datasets have been deposited in the Gene Expression Omnibus (GSE213305). Data supporting the plots within this article and other findings of this study are available from the corresponding author upon request. 

Supplemental data

This article contains [supplemental data](#).

Acknowledgments

The authors thank all lab members for their technical assistance and Dr Wenxin Zhao for preparing recombinant AlkB.

Author contributions

R. H. and C. Z. conceptualization; R. H., J. S., J. L., and X. L. methodology; T. Z. and J. S. software; R. H., J. L., and X. L. validation; R. H., J. S., J. L., X. L., J. W., T. Z., and C. Z. formal analysis; R. H., J. S., J. L., X. L., J. W., L. Z., and Q. C. investigation; L. Z. and Q. C. resources; R. H., J. S., and T. Z. data curation; R. H., J. S., L. Z., T. Z., Q. C., and C. Z. writing—original draft; R. H., J. S., T. Z., Q. C., and C. Z. writing—review & editing; R. H., J. S., T. Z., Q. C., and C. Z. visualization; Q. C. and C. Z. supervision; C. Z. project administration; T. Z., Q. C., and C. Z. funding acquisition.

Author ORCIDs

Jake Wu  <https://orcid.org/0000-0003-4004-7180>

Linlin Zhao  <https://orcid.org/0000-0002-8821-4198>

Funding and additional information

This work was supported in part by the National Institutes of Health grants (R01HL167206, R01HL131925, R01ES023470, R01ES032024, and R35GM128854) and an American Heart Association grant (grant no.: 19TPA34890065). R. H. was supported by a National Institutes of Health National Research Service Award T32 training grant (grant no.:

T32ES018827) and an American Heart Association predoctoral fellowship (grant no.: 23PRE1018751). The content is solely the responsibility of the authors and does not necessarily represent the official views of the National Institutes of Health and American Heart Association.

Conflict of interest

The authors declare that they have no conflicts of interest with the contents of this article.

Abbreviations

BCA, brachiocephalic artery; cDNA, complementary DNA; DEG, differentially expressed gene; FAIME, Functional Analysis of Individual Microarray Expression; FC, fold change; FDR, false discovery rate; HCD, high-cholesterol diet; KEGG, Kyoto Encyclopedia of Genes and Genomes; LCD, low-cholesterol diet; LDLR, LDL receptor; miRNA, microRNA; ncRNA, noncoding RNA; PANDORA-Seq, Panoramic RNA Display by Overcoming RNA Modification Aborted Sequencing; piRNA, piwi-interacting RNA; RNA-Seq, RNA sequencing; rsRNA, ribosomal RNA-derived small RNA; SMC, smooth muscle cell; sncRNA, small non-coding RNA; tsRNA, transfer RNA-derived small RNA.

Manuscript received September 2, 2022, and in revised form February 8, 2023. Published, JLR Papers in Press, March 4, 2023, <https://doi.org/10.1016/j.jlr.2023.100352>

REFERENCES

- Libby, P. (2002) Inflammation in atherosclerosis. *Nature*. **420**, 868–874
- Libby, P., Ridker, P. M., and Maseri, A. (2002) Inflammation and atherosclerosis. *Circulation*. **105**, 1135–1143
- Sage, A. P., and Mallat, Z. (2017) Readapting the adaptive immune response - therapeutic strategies for atherosclerosis. *Br. J. Pharmacol.* **174**, 3926–3939
- Hansson, G. K. (2017) Inflammation and atherosclerosis: the end of a controversy. *Circulation*. **136**, 1875–1877
- Lu, W., Park, S. H., Meng, Z., Wang, F., and Zhou, C. (2019) Deficiency of adipocyte IKKbeta affects atherosclerotic plaque vulnerability in obese LDLR deficient mice. *J. Am. Heart Assoc.* **8**, e012009
- Gimbrone, M. A., and García-Cardena, G. (2016) Endothelial Cell dysfunction and the pathobiology of atherosclerosis. *Circ. Res.* **118**, 620–636
- Hernandez, R., and Zhou, C. (2021) Recent advances in understanding the role of IKKbeta in cardiometabolic diseases. *Front. Cardiovasc. Med.* **8**, 752337
- Ferreira, V., van Dijk, K. W., Groen, A. K., Vos, R. M., van der Kaa, J., Gijbels, M. J., et al. (2007) Macrophage-specific inhibition of NF-kappaB activation reduces foam-cell formation. *Atherosclerosis*. **192**, 283–290
- Park, S. H., Sui, Y., Gizard, F., Xu, J., Rios-Pilier, J., Hellsley, R. N., et al. (2012) Myeloid-specific IkappaB kinase beta deficiency decreases atherosclerosis in low-density lipoprotein receptor-deficient mice. *Arterioscler. Thromb. Vasc. Biol.* **32**, 2869–2876
- Lusis, A. J. (2000) Atherosclerosis. *Nature*. **407**, 233–241
- Sui, Y., Park, S. H., Hellsley, R. N., Sunkara, M., Gonzalez, F. J., Morris, A. J., et al. (2014) Bisphenol A increases atherosclerosis in pregnane X receptor-humanized ApoE deficient mice. *J. Am. Heart Assoc.* **3**, e000492
- Liu, J., Hernandez, R., Li, X., Meng, Z., Chen, H., and Zhou, C. (2022) Pregnane X receptor mediates atherosclerosis induced by dicyclohexyl phthalate in LDL receptor-deficient mice. *Cells*. **11**, 1125
- Hellsley, R. N., and Zhou, C. (2017) Epigenetic impact of endocrine disrupting chemicals on lipid homeostasis and atherosclerosis: a pregnane X receptor-centric view. *Environ. Epigenet.* **3**, dvx017
- Lind, L., Araujo, J. A., Barchowsky, A., Belcher, S., Berridge, B. R., Chiamvimonvat, N., et al. (2021) Key characteristics of cardiovascular toxicants. *Environ. Health Perspect.* **129**, 95001
- Wei, T., Liu, J., Zhang, D., Wang, X., Li, G., Ma, R., et al. (2021) The Relationship between nutrition and atherosclerosis. *Front. Bioeng. Biotechnol.* **9**, 635504
- Das, S., Shah, R., Dimmeler, S., Freedman, J. E., Holley, C., Lee, J. M., et al. (2020) Noncoding RNAs in cardiovascular disease: current knowledge, tools and technologies for investigation, and future directions: a scientific statement from the American heart association. *Circ. Genom. Precis. Med.* **13**, e000062
- Lu, Y., Thavarajah, T., Gu, W., Cai, J., and Xu, Q. (2018) Impact of miRNA in Atherosclerosis. *Arterioscler. Thromb. Vasc. Biol.* **38**, e159–e170
- Feinberg, M. W., and Moore, K. J. (2016) MicroRNA regulation of atherosclerosis. *Circ. Res.* **118**, 703–720
- Wysoczynski, M., Kim, J., Moore, J. B., and Uchida, S. (2020) Macrophage long non-coding RNAs in Pathogenesis of cardiovascular disease. *Noncoding RNA*. **6**, 28
- Simon, V., Zhou, H., Pierce, J. B., Yang, D., Haemmig, S., Tesmenitsky, Y., et al. (2020) LncRNA VINAS regulates atherosclerosis by modulating NF-κB and MAPK signaling. *JCI Insight*. **5**, e140627
- Shi, J., Zhou, T., and Chen, Q. (2022) Exploring the expanding universe of small RNAs. *Nat. Cell Biol.* **24**, 415–423
- Shi, J., Zhang, Y., Tan, D., Zhang, X., Yan, M., Zhang, Y., et al. (2021) PANDORA-seq expands the repertoire of regulatory small RNAs by overcoming RNA modifications. *Nat. Cell Biol.* **23**, 424–436
- Rigoutsos, I., Londin, E., and Kirino, Y. (2019) Short RNA regulators: the past, the present, the future, and implications for precision medicine and health disparities. *Curr. Opin. Biotechnol.* **58**, 202–210
- Quintana, J. F., Kumar, S., Ivens, A., Chow, F. W. N., Hoy, A. M., Fulton, A., et al. (2019) Comparative analysis of small RNAs released by the filarial nematode *Litomosoides sigmodontis* in vitro and in vivo. *PLoS Negl. Trop. Dis.* **13**, e0007811
- Hoen, E. N. M., Buermans, H. P. J., Waasdorp, M., Stoorvogel, W., Wauben, M. H. M., and Hoen, P. A. C. (2012) Deep sequencing of RNA from immune cell-derived vesicles uncovers the selective incorporation of small non-coding RNA biotypes with potential regulatory functions. *Nucleic Acids Res.* **40**, 9272–9285
- Sergiev, P. V., Aleksashin, N. A., Chugunova, A. A., Polikanov, Y. S., and Dontsova, O. A. (2018) Structural and evolutionary insights into ribosomal RNA methylation. *Nat. Chem. Biol.* **14**, 226–235
- Phizicky, E. M., and Hopper, A. K. (2010) tRNA biology charges to the front. *Genes Dev.* **24**, 1832–1860
- Schimmel, P. (2018) The emerging complexity of the tRNA world: mammalian tRNAs beyond protein synthesis. *Nat. Rev. Mol. Cell Biol.* **19**, 45–58
- Honda, S., Loher, P., Shigematsu, M., Palazzo, J. P., Suzuki, R., Imoto, I., et al. (2015) Sex hormone-dependent tRNA halves enhance cell proliferation in breast and prostate cancers. *Proc. Natl. Acad. Sci. U. S. A.* **112**, E3816–3825
- [preprint] Akiyama, Y., Lyons, S. M., Fay, M. M., Abe, T., Anderson, P., and Ivanov, P. (2019) Multiple ribonuclease A family members cleave transfer RNAs in response to stress. *bioRxiv*. <https://doi.org/10.1101/811174>
- Shigematsu, M., Kawamura, T., and Kirino, Y. (2018) Generation of 2',3'-Cyclic Phosphate-Containing RNAs as a Hidden Layer of the Transcriptome. *Front. Genet.* **9**, 562
- Zheng, G., Qin, Y., Clark, W. C., Dai, Q., Yi, C., He, C., et al. (2015) Efficient and quantitative high-throughput tRNA sequencing. *Nat. Met.* **12**, 835–837
- Cozen, A. E., Quartley, E., Holmes, A. D., Hrabeta-Robinson, E., Phizicky, E. M., and Lowe, T. M. (2015) ARM-seq: AlkB-facilitated RNA methylation sequencing reveals a complex landscape of modified tRNA fragments. *Nat. Met.* **12**, 879–884
- Liu, J., Shi, J., Hernandez, R., Li, X., Konchadi, P., Miyake, Y., et al. (2023) Paternal phthalate exposure-elicited offspring metabolic disorders are associated with altered sperm small RNAs in mice. *Environ. Int.* **172**, 107769
- Teupser, D., Persky, A. D., and Breslow, J. L. (2003) Induction of atherosclerosis by low-fat, semisynthetic diets in LDL receptor-

- deficient C57BL/6J and FVB/NJ mice: comparison of lesions of the aortic root, brachiocephalic artery, and whole aorta (in face measurement). *Arterioscler. Thromb. Vasc. Biol.* **23**, 1907–1913
36. Meng, Z., Hernandez, R., Liu, J., Gwag, T., Lu, W., Hsiai, T. K., et al. (2022) HIV protein tat induces macrophage dysfunction and atherosclerosis development in low-density lipoprotein receptor-deficient mice. *Cardiovasc. Drugs Ther.* **36**, 201–215
 37. Sui, Y., Park, S. H., Xu, J., Monette, S., Hsley, R. N., Han, S. S., et al. (2014) IKKbeta links vascular inflammation to obesity and atherosclerosis. *J. Exp. Med.* **211**, 869–886
 38. Robinet, P., Milewicz, D. M., Cassis, L. A., Leeper, N. J., Lu, H. S., and Smith, J. D. (2018) Consideration of sex differences in design and reporting of experimental arterial pathology studies—statement from ATVB council. *Arterioscler. Thromb. Vasc. Biol.* **38**, 292–303
 39. Lu, W., Meng, Z., Hernandez, R., and Zhou, C. (2021) Fibroblast-specific IKK-beta deficiency ameliorates angiotensin II-induced adverse cardiac remodeling in mice. *JCI Insight* **6**, e150161
 40. Sui, Y., Meng, Z., Chen, J., Liu, J., Hernandez, R., Gonzales, M. B., et al. (2021) Effects of dicyclohexyl phthalate exposure on PXR activation and lipid homeostasis in mice. *Environ. Health Perspect.* **129**, 127001
 41. Hsley, R. N., Sui, Y., Park, S. H., Liu, Z., Lee, R. G., Zhu, B., et al. (2016) Targeting IkappaB kinase beta in adipocyte lineage cells for treatment of obesity and metabolic dysfunctions. *Stem Cells* **34**, 1883–1895
 42. Satta, S., Meng, Z., Hernandez, R., Cavallero, S., Zhou, T., Hsiai, T. K., et al. (2022) An engineered nano-liposome-human ACE2 decoy neutralizes SARS-CoV-2 Spike protein-induced inflammation in both murine and human macrophages. *Theranostics* **12**, 2639–2657
 43. Havel, R. J., Eder, H. A., and Bragdon, J. H. (1955) The distribution and chemical composition of ultracentrifugally separated lipoproteins in human serum. *J. Clin. Invest.* **34**, 1345–1353
 44. Wang, F., Liu, Z., Park, S. H., Gwag, T., Lu, W., Ma, M., et al. (2018) Myeloid beta-catenin deficiency exacerbates atherosclerosis in low-density lipoprotein receptor-deficient mice. *Arterioscler. Thromb. Vasc. Biol.* **38**, 1468–1478
 45. Sui, Y., Meng, Z., Park, S. H., Lu, W., Livel, C., Chen, Q., et al. (2020) Myeloid-specific deficiency of pregnane X receptor decreases atherosclerosis in LDL receptor-deficient mice. *J. Lipid Res.* **61**, 696–706
 46. Wong, T. W. Y., Ahmed, A., Yang, G., Maino, E., Steiman, S., Hyatt, E., et al. (2020) A novel mouse model of Duchenne muscular dystrophy carrying a multi-exonic. *Dis. Model Mech.* **13**, dmm045369
 47. Pickering, R. J., Tikellis, C., Rosado, C. J., Tsorotes, D., Dimitropoulos, A., Smith, M., et al. (2019) Transactivation of RAGE mediates angiotensin-induced inflammation and atherogenesis. *J. Clin. Invest.* **129**, 406–421
 48. Ivanov, P., Emara, M. M., Villen, J., Gygi, S. P., and Anderson, P. (2011) Angiogenin-induced tRNA fragments inhibit translation initiation. *Mol. Cell* **43**, 613–623
 49. Sun, X., He, S., Wara, A. K. M., Icli, B., Shvartz, E., Tesmenitsky, Y., et al. (2014) Systemic delivery of microRNA-181b inhibits nuclear factor- κ B activation, vascular inflammation, and atherosclerosis in apolipoprotein E-deficient mice. *Circ. Res.* **114**, 32–40
 50. Robinson, M. D., McCarthy, D. J., and Smyth, G. K. (2010) edgeR: a Bioconductor package for differential expression analysis of digital gene expression data. *Bioinformatics* **26**, 139–140
 51. Levin, J. Z., Yassour, M., Adiconis, X., Nusbaum, C., Thompson, D. A., Friedman, N., et al. (2010) Comprehensive comparative analysis of strand-specific RNA sequencing methods. *Nat. Met.* **7**, 709–715
 52. Zhong, S., Joung, J. G., Zheng, Y., Chen, Y. R., Liu, B., Shao, Y., et al. (2011) High-throughput illumina strand-specific RNA sequencing library preparation. *Cold Spring Harb. Protoc.* **2011**, 940–949
 53. Yang, X., Regan, K., Huang, Y., Zhang, Q., Li, J., Seiwert, T. Y., et al. (2012) Single sample expression-anchored mechanisms predict survival in head and neck cancer. *PLoS Comput. Biol.* **8**, e1002350
 54. Zhou, C., King, N., Chen, K. Y., and Breslow, J. L. (2009) Activation of PXR induces hypercholesterolemia in wild-type and accelerates atherosclerosis in apoE deficient mice. *J. Lipid Res.* **50**, 2004–2013
 55. Sui, Y., Xu, J., Rios-Pilier, J., and Zhou, C. (2011) Deficiency of PXR decreases atherosclerosis in apoE-deficient mice. *J. Lipid Res.* **52**, 1652–1659
 56. Shi, J., Ko, E. A., Sanders, K. M., Chen, Q., and Zhou, T. (2018) SPORTS1.0: a tool for annotating and profiling non-coding RNAs optimized for rRNA- and tRNA-derived small RNAs. *Genomics Proteomics Bioinform.* **16**, 144–151
 57. Chen, Q., Zhang, X., Shi, J., Yan, M., and Zhou, T. (2021) Origins and evolving functionalities of tRNA-derived small RNAs. *Trends Biochem. Sci.* **46**, 790–804
 58. Ozata, D. M., Gainetdinov, I., Zoch, A., O'Carroll, D., and Zamore, P. D. (2019) PIWI-interacting RNAs: small RNAs with big functions. *Nat. Rev. Genet.* **20**, 89–108
 59. Bartel, D. P. (2018) Metazoan MicroRNAs. *Cell* **173**, 20–51
 60. Kumar, P., Kuscu, C., and Dutta, A. (2016) Biogenesis and function of Transfer RNA-Related Fragments (tRFs). *Trends Biochem. Sci.* **41**, 679–689
 61. Lambert, M., Benmoussa, A., and Provost, P. (2019) Small non-coding RNAs derived from eukaryotic ribosomal RNA. *Non-coding RNA* **5**, 16
 62. Hrabeta-Robinson, E., Marcus, E., Cozen, A. E., Phizicky, E. M., and Lowe, T. M. (2017) High-throughput small RNA sequencing enhanced by AlkB-facilitated RNA de-methylation (ARM-Seq). *Met. Mol. Biol.* **1562**, 231–243
 63. Wang, L. K., Lima, C. D., and Shuman, S. (2002) Structure and mechanism of T4 polynucleotide kinase: an RNA repair enzyme. *EMBO J.* **21**, 3873–3880
 64. Busnelli, M., Manzini, S., Chiara, M., Colombo, A., Fontana, F., Oleari, R., et al. (2021) Aortic gene expression profiles show how ApoA-I levels modulate inflammation, lysosomal activity, and sphingolipid metabolism in murine atherosclerosis. *Arterioscler. Thromb. Vasc. Biol.* **41**, 651–667
 65. Xi, D., Zhao, J., Zhao, M., Fu, W., Guo, Z., and Chen, H. (2017) Identification of gene expression changes in the aorta of apoE null mice fed a high-fat diet. *Genes (Basel)* **8**, 289
 66. He, X., Yang, Y., Wang, Q., Wang, J., Li, S., Li, C., et al. (2021) Expression profiles and potential roles of transfer RNA-derived small RNAs in atherosclerosis. *J. Cell Mol. Med.* **25**, 7052–7065
 67. Borång, S., Andersson, T., Thelin, A., Odeberg, J., and Lundberg, J. (2004) Vascular gene expression in atherosclerotic plaque-prone regions analyzed by representational difference analysis. *Pathobiology* **71**, 107–114
 68. Moore, K. J., and Tabas, I. (2011) Macrophages in the pathogenesis of atherosclerosis. *Cell* **145**, 341–355
 69. Lin, J., Kakkar, V., and Lu, X. (2014) Impact of MCP-1 in atherosclerosis. *Curr. Pharm. Des.* **20**, 4580–4588
 70. Moos, M. P., John, N., Gräßner, R., Nossmann, S., Günther, B., Vollandt, R., et al. (2005) The lamina adventitia is the major site of immune cell accumulation in standard chow-fed apolipoprotein E-deficient mice. *Arterioscler. Thromb. Vasc. Biol.* **25**, 2386–2391
 71. Wang, I. M., Zhang, B., Yang, X., Zhu, J., Stepaniants, S., Zhang, C., et al. (2012) Systems analysis of eleven rodent disease models reveals an inflammatome signature and key drivers. *Mol. Syst. Biol.* **8**, 594
 72. Berisha, S. Z., Hsu, J., Robinet, P., and Smith, J. D. (2013) Transcriptome analysis of genes regulated by cholesterol loading in two strains of mouse macrophages associates lysosome pathway and ER stress response with atherosclerosis susceptibility. *PLoS One* **8**, e65003
 73. Raitoharju, E., Lyytikäinen, L. P., Levula, M., Oksala, N., Mennander, A., Tarkka, M., et al. (2011) miR-21, miR-210, miR-34a, and miR-146a/b are up-regulated in human atherosclerotic plaques in the Tampere Vascular Study. *Atherosclerosis* **219**, 211–217
 74. Takahashi, Y., Satoh, M., Minami, Y., Tabuchi, T., Itoh, T., and Nakamura, M. (2010) Expression of miR-146a/b is associated with the Toll-like receptor 4 signal in coronary artery disease: effect of renin-angiotensin system blockade and statins on miRNA-146a/b and Toll-like receptor 4 levels. *Clin. Sci.* **119**, 395–405
 75. Suárez, Y., Wang, C., Manes, T. D., and Pober, J. S. (2010) Cutting edge: TNF-induced microRNAs regulate TNF-induced expression of E-selectin and intercellular adhesion molecule-1 on human endothelial cells: feedback control of inflammation. *J. Immunol.* **184**, 21–25

76. Liu, D., Dejun, L., Sun, X., Xuelin, S., Ye, P., and Ping, Y. (2015) miR-31 Overexpression exacerbates atherosclerosis by targeting NOX4 in apoE(-/-) mice. *Clin. Lab.* **61**, 1617–1624
77. Sun, X., Belkin, N., and Feinberg, M. W. (2013) Endothelial microRNAs and atherosclerosis. *Curr. Atheroscler. Rep.* **15**, 372
78. Shi, J., Zhang, Y., Zhou, T., and Chen, Q. (2019) tsRNAs: the swiss army knife for translational regulation. *Trends Biochem. Sci.* **44**, 185–189
79. Xie, Y., Yao, L., Yu, X., Ruan, Y., Li, Z., and Guo, J. (2020) Action mechanisms and research methods of tRNA-derived small RNAs. *Signal. Transduct. Target. Ther.* **5**, 109
80. Wen, J. T., Huang, Z. H., Li, Q. H., Chen, X., Qin, H. L., and Zhao, Y. (2021) Research progress on the tsRNA classification, function, and application in gynecological malignant tumors. *Cell Death Discov.* **7**, 388
81. Li, X., Liu, X., Zhao, D., Cui, W., Wu, Y., Zhang, C., *et al.* (2021) tRNA-derived small RNAs: novel regulators of cancer hallmarks and targets of clinical application. *Cell Death Discov.* **7**, 249
82. Chen, Q., Yan, M., Cao, Z., Li, X., Zhang, Y., Shi, J., *et al.* (2016) Sperm tsRNAs contribute to intergenerational inheritance of an acquired metabolic disorder. *Science.* **351**, 397–400
83. Zhang, Y., Zhang, X., Shi, J., Tuorto, F., Li, X., Liu, Y., *et al.* (2018) Dnmt2 mediates intergenerational transmission of paternally acquired metabolic disorders through sperm small non-coding RNAs. *Nat. Cell Biol.* **20**, 535–540
84. Kim, H. K., Fuchs, G., Wang, S., Wei, W., Zhang, Y., Park, H., *et al.* (2017) A transfer-RNA-derived small RNA regulates ribosome biogenesis. *Nature* **552**, 57–62
85. Zhang, X., Cozen, A. E., Liu, Y., Chen, Q., and Lowe, T. M. (2016) Small RNA modifications: integral to function and disease. *Trends Mol. Med.* **22**, 1025–1034